Geosci. Model Dev. Discuss., 8, 5437–5479, 2015
www.geosci-model-dev-discuss.net/8/5437/2015/
doi:10.5194/gmdd-8-5437-2015

Geoscientific Model Development Discussions
Open Access

Sensitivity of the WRF model to PBL parametrizations and nesting techniques: evaluation of surface wind over complex terrain

J. J. Gómez-Navarro[1,2], C. C. Raible[1,2], and S. Dierer[3]

[1]Climate and Environmental Physics, Physics Institute, University of Bern, Sidlerstrasse 5, 3012 Bern, Switzerland
[2]Oeschger Centre for Climate Change Research, Sidlerstrasse 5, 3012 Bern, Switzerland
[3]Axis, Brandschenkestrasse 90, 8002 Zurich, Switzerland

Received: 13 May 2015 – Accepted: 25 June 2015 – Published: 15 July 2015

Correspondence to: J. J. Gómez-Navarro (gomez@climate.unibe.ch)

Published by Copernicus Publications on behalf of the European Geosciences Union.

Abstract

Simulating surface wind over complex terrain is a challenge in regional climate modelling. Therefore, this study aims at identifying a setup of the WRF model that minimizes systematic errors of surface winds in hindcast simulations. Major factors of the model configuration are tested to find a suitable setup: the horizontal resolution, the PBL parameterization scheme and the way WRF is nested to the driving dataset. Hence, a number of sensitivity simulations at a spatial resolution of 2 km are carried out and compared to observations. Given the importance of wind storms, the analysis is based on case studies of 24 historical wind storms that caused great economic damage in Switzerland. Each of these events is downscaled using eight different model setups, but sharing the same driving dataset. The results show that the unresolved topography leads to a general overestimation of wind speed in WRF. However, this bias can be substantially reduced by using a PBL scheme that explicitly considers the effects of non-resolved topography, which also improves the spatial structure of wind speed over Switzerland. The wind direction, although generally well reproduced, is not very sensitive to the PBL scheme. Further sensitivity tests include four types of nesting methods: nesting only at the boundaries of the outermost domain, analysis and spectral nudging, and the so-called re-forecast method, where the simulation is frequently restarted. These simulations show that restricting the freedom of the model to develop large-scale disturbances slightly increases the temporal agreement with the observations, at the same time that it further reduces the overestimation of wind speed, especially for maximum wind peaks. The model skill is also evaluated in the outermost domains, where the resolution is coarser. The results demonstrate the important role of horizontal resolution, where the step from 6 to 2 km significantly improves model performance. In summary, the combination of a grid size of 2 km, the non-local PBL scheme modified to explicitly account for non-resolved orography, as well as analysis or spectral nudging, is a superior combination when dynamical downscaling is aimed at reproducing real wind fields.

1 Introduction

Prominent features of the North Atlantic and European climate are cyclonic disturbances, which may be intensified and lead to severe storms (von Storch and Weisse, 2008). Several severe wind storms have hit Central Europe during the last decades (Schiesser et al., 1997; Etienne et al., 2013). These events, although rare, produce considerable economical cost and are listed as an important natural hazard in Europe (Beniston et al., 2007). Ongoing economic and demographic growth, as well as climate change may imply even stronger impacts in the future, which has raised concerns among reinsurance companies, since isolated events such as storm Lothar in December 1999 caused damages of up to USD 12 billion (MunichRe, 2001). A better understanding of the mechanisms leading to severe wind storms, and a reliable projection of their characteristics under climate change conditions is important to minimize the impact of such events in contemporary and future societies (Muskulus and Jacob, 2005; Goyette, 2010). However, wind is still not as widely studied as temperature or precipitation (e.g. Schär et al., 2004; Kjellström et al., 2007; Rajczak et al., 2013). For example in areas of complex terrain like Switzerland the main focus of high resolution simulations with respect to wind is on case studies (Goyette, 2008; Etienne et al., 2013). Recently, simulations of about 90 storms over Switzerland are combined to a storm climatology (Welker et al., 2015).

The fundamental problem regarding surface wind is its intrinsically complex nature, particularly over areas of complex terrain like the Alps (Whiteman, 2000). This complexity precludes its realistic simulation with coarse-resolution models, but also hampers the extrapolation of local observations onto regular grids, which could be used for impact studies. Dynamical downscaling is a common tool that allows bridging the gap between the coarse resolution of Global Circulation Models (GCMs) or reanalysis products and the local terrain characteristics that influence temperature, precipitation or wind (e.g., Kotlarski et al., 2014). Thereby, this method employs Regional Climate Models (RCMs), which, driven at the boundaries by a global dataset, simulate the climate in a limited area domain. This reduces computational costs, which in turn allows implementing simulations with higher spatial resolutions. RCMs driven by GCMs are used for a variety of applications: from climate change projections (Kjellström et al., 2007; van der Linden and Mitchell, 2009; Gómez-Navarro et al., 2010; Jerez et al., 2013; Rajczak et al., 2013; Jacob et al., 2013) to paleoclimatology (Gómez-Navarro et al., 2013, and references therein). Besides, they are used in the so-called hindcast simulations, which blend the reliability of reanalysis products with the high-resolution provided by RCMs. Studies focusing specifically on wind have been one of the applications of such type of simulations (Jiménez et al., 2010; Jerez and Trigo, 2013; Etienne et al., 2013; García-Díez et al., 2013; Menendez et al., 2014; Lorente-Plazas et al., 2014a; Draxl et al., 2014).

RCMs, however, contain various sources of uncertainties, like deviations in the driving dataset, numerical approximations, as well as parametrizations of the sub-grid processes. A number of studies in different locations assessed the sensitivity of the model performance due to different model configurations. Dierer et al. (2005) studied the dependency of wind speed on the Planetary Boundary Layer (PBL) parameterizations implemented in the model MM5 as well as the atmospheric stability in different European countries. More recently, García-Díez et al. (2013) focused on the role of different PBL schemes. Other studies have investigated the role of the PBL schemes in the ability of simulating surface wind of typhoons (Kwun et al., 2009), along the coast of the Mediterranean Sea (Menendez et al., 2014), or in Southern Spain (Santos-Alamillos et al., 2013).

Although the studies discussed above tackle the problem of the uncertainties in the model configuration regarding wind, they do not focus on areas of complex topography. As suggested by Jiménez et al. (2008), in such areas the spatial resolution becomes a major challenge, and the conclusions drawn from coarser resolution simulations cannot be generalised without caution. Thus, the present study aims at finding a model setup that minimises systematic errors in hindcast simulations in storms with the purpose of reproducing mean and maximum surface winds in complex terrains. Thereby, potentially important sensitivities of the model setup are explored, which encompass spatial resolution, PBL parameterizations and the use of nudging techniques. The sensitivity with respect to the driving data set is not investigated in order to concentrate on the sensitivity within the model. Geographically the study focuses on the Alpine area. Since the simulations at 2 km grid size require significant computational power, the study is based on a case study approach, rather than continuous simulations. Hence, a total of 24 historical wind storms is simulated for each model setup.

The study is structured as follows: Sect. 2 presents the reanalysis product used to drive the RCM and the observational network. Section 3 describes the model setup including the different nesting options tested in this study. It further presents the set of sensitivity experiments carried out. The results are discussed in Sect. 4 focusing first on the role of the PBL scheme and the nesting method applied. Then, the role of the horizontal resolution is discussed, including how errors are spatially distributed over different areas of the Alps. Finally, Sect. 5 draws main conclusions.

2 Data

2.1 Reanalysis dataset

The dataset providing the initial and boundary conditions for the RCM is the ERA-Interim reanalysis (Dee et al., 2011). It spans the period from 1979 to today, and is used in its highest resolution of $0.75^{\circ} \times 0.75^{\circ}$. The ERA-Interim dataset is generated by running the Integrated Forecast System model (version 2006) of the European Centre for Medium-Range Weather Forecasts (ECMWF). The horizontal resolution of the model is T255 (approximately 80 km). The model has 60 vertical levels up to a pressure level of 0.1 hPa. Observational data are assimilated with a 4-dimensional variational analysis (4D-Var) in a 12 h analysis window. A number of observational datasets are used ranging from satellite data to surface pressure observations and radiosonde profiles (Dee et al., 2011). However, the assimilation system does not take into account obser-

GMDD
8, 5437–5479, 2015
Sensitivity of WRF to reproduce surface wind over complex terrain
J. J. Gómez-Navarro et al.

vations of surface wind, which is important to avoid circularity given that this study uses wind observations in the validation part, neither observations of pressure and humidity over high terrain (typically elevations higher than 1500 m).

2.2 Observational data

To evaluate the model's ability in dynamically downscaling wind storms, a reliable set of observations is required. In particular, this is the case in areas of complex terrain, where wind speed and direction can vary within distances of tens of meters. The Swiss Federal Office of Meteorology and Climatology (MeteoSwiss) provides such observations from a dense network of weather stations. This dataset contains 10 min mean values of wind speed and direction. The model simulations are evaluated hereafter by using hourly means of weather station wind measurements calculated from their 10 min mean.

Some basic data checks are carried out before using the data in the evaluation. Following an approach similar to Lorente-Plazas et al. (2014b), all series are visually inspected. Simple plausibility checks are performed, such as calculating and plotting the running mean and standard deviation to search for anomalies. Stations showing spurious jumps or gaps are discarded from the analysis hereafter. The measurement heights above ground differ. Therefore, the simulated wind is linearly interpolated to the measurement height for the comparison with observations. After the quality checks, the remaining weather station network still sufficiently covers Switzerland (Fig. 1). We consider in the analysis all the stations that recorded each individual storm. Note that this number increases with time as the observational network has been growing. Thereby, the first storm selected took place in February 1990, and was recorded by a total of 68 stations and the last storm in February 2010 was recorded by 112 stations. 65 stations capture all 24 storms, 36 missed just one storm, whereas only 4 sites captured less than 20 storms. The weather stations cover a wide variety of geographical conditions: plains, valleys and mountainous areas with a minimum (maximum) height of 197 (3580) m a.s.l. Thus, this dataset allows evaluating surface wind simulations under

GMDD
8, 5437–5479, 2015

different geographical and climatic conditions. Still, as suggested by Gómez-Navarro et al. (2012), the errors and uncertainties contained in the observations shall not be neglected, but need to be kept in mind when using it to draw conclusions about simulation performance.

3 Model and experimental design

3.1 Model setup

The study is based on the Weather Research and Forecasting Model (WRF, version 3.5), aired in September 2013 (Skamarock et al., 2008). WRF is a limited area meteorological model used for weather forecasting and climatic purposes. It employs an Eulerian mass-coordinate solver with a non-hydrostatic approach, and a terrain following eta-coordinate system in the vertical. It is a state-of-the-art mesoscale model used in a variety of studies also for hindcast simulations (Kwun et al., 2009; Jiménez et al., 2010, 2012; Awan et al., 2011; García-Díez et al., 2013; Jiménez and Dudhia, 2013; Santos-Alamillos et al., 2013; Menendez et al., 2014, among others).

A first decision in regional climate modelling concerns the selection of the domain to be simulated. Although this selection is susceptible of introducing uncertainties, this study employs just one domain setup, and hence the sensitivity of the performance to the model domain is not investigated here. There are a number of reasons for this. First, there is not much freedom, in the sense that the domain is primary selected according to the area of interest, in this case the Alpine area. The number of domains is conditioned by the resolution of the driving data set and the final resolution of 2 km aimed in our study. So only one is used in all simulations (Fig. 2). It consists of four two-way nested domains with grid size of 54, 18, 6 and 2 km for the domains D1 to D4, respectively. All domain use a Lambert conformal projection, which conserves the spatial distances in both directions. The analysis hereafter evaluates the model skill with the focus set on the innermost domain, although the model performance in the coarser domains is also investigated to assess the role of the horizontal resolution. Vertically, WRF does not allow using a varying number of levels in nested domains. Hence, the number of vertical levels has been set to 40 in every domain. This number is similar to the number in recent literature, which ranges between 30 and 46 (Miguez-Macho et al., 2004; Lo et al., 2008; Kwun et al., 2009; Jiménez and Dudhia, 2012; Santos-Alamillos et al., 2013; Etienne et al., 2013). The vertical resolution ensures that several eta levels lie below the PBL height at any time. Naturally, the number of levels within the PBL varies at each grid point according to the PBL height due to different meteorological situations. In the simulations carried out, a minimum (maximum) of 3 (7) levels vertical layers lie within the PBL at any time.

Another source of uncertainty is related to the choice of the physical parameterizations, such as microphysics, convection, radiation and the formation of the PBL, among others (Stensrud, 2007). Since the latter is the parameterization that is most relevant for the surface winds, a number of sensitivity tests are conducted and analysed in order to find the most appropriate PBL scheme (see next section). The other parameterizations remain unchanged in all simulations, i.e., the Microphysics WRF Single Moment 6-class scheme (Hong and Lim, 2006), the Kain–Fritsch scheme of cumulus (Kain, 2004), which is implemented only in the two outermost domains, the Rapid and accurate Radiative Transfer Model (RRTM) (Mlawer et al., 1997), the short-wave radiation scheme by Dudhia (1989), and the Noah land soil model (Chen and Dudhia, 2001).

3.2 PBL schemes

The PBL plays a major role in simulating surface winds (Stensrud, 2007; Kwun et al., 2009; Santos-Alamillos et al., 2013; Menendez et al., 2014). Nowadays, there are many different approximations to account for the relevant subgrid processes that lead to different PBL formations. In this study four different schemes are implemented, which capture a considerable range of different approaches possible. Similar to García-Díez et al. (2013), we use the fully non-local scheme developed in the Yonsei University (hereafter YSU) (Hong and Lim, 2006), the local closure scheme by Mellor–Yamada–

Janjic (MYJ) (Mellor and Yamada, 1982; Janjić, 2001), and the Asymmetric Convective Model 2 (ACM2), which combines local and non-local transport depending on the atmosphere conditions (Pleim, 2007a, b). García-Díez et al. (2013) described the different approaches in detail, therefore not repeated here. The fourth scheme is a subtle modification of the YSU scheme that accounts for the unresolved orography by introducing a correction term in the momentum equation (Jiménez and Dudhia, 2012). This scheme aims at correcting a general problem of WRF with simulating wind, namely its tendency to overestimate wind speed (Cheng and Steenburgh, 2005; Mass and Ovens, 2011; Jiménez and Dudhia, 2012). This is in particular a problem in areas of complex terrain, where topographic features not explicitly considered by the coarse resolution of the model introduce further friction. This scheme is referred hereafter as YSU*.

3.3 Nesting approach

RCMs are nested in a global dataset, which drives the simulation by providing the initial and boundary conditions. Dynamical downscaling is hence mostly an initial value problem in the first days of the simulation, which evolves into a boundary value problem when the initial state has been "forgotten" by the atmosphere. However, how to specify the lateral boundary conditions is a mathematically ill-posed problem, since they become over-specified (Staniforth, 1997). A solution to this problem, widely adopted in state-of-the-art RCMs, consists of newtonially relaxing the driving fields in a buffer zone around the borders of the grid (Davies, 1976). This relaxation damps small scale discrepancies, but does not handle large-scales properly and generates disturbances in the large-scale circulation (Miguez-Macho et al., 2005). Several methods have been proposed to deal with this problem.

The first approach basically consists of using Newtonian relaxation at the boundaries without any correction inside the domains. This is referred hereafter as "free simulations". In favour of this approach, it is argued that simulations benefit from a better representation and the undisturbed development of regional processes. Another argument is that RCMs are often used to downscale climate change projections or paleosimulations. Such simulations are performed with relatively coarse GCMs, so that modifications of the large-scale circulation maybe beneficial, as potential biases from the GCMs may be partly corrected by the RCMs.

In case of reanalysis data used at the boundaries, it may be desirable that the RCM simulation stays close to the large-scale situation of the driving data. A first method to achieve this is the so-called reforecast simulation. The method consists of splitting a long simulation in shorter simulation periods of one to few days, running each period separately and finally merging them. This method effectively minimises the impact of the boundaries, transforming the problem into a mostly initial-value problem. The reforecast method is regularly applied (Jiménez and Dudhia, 2012; García-Díez et al., 2013; Menendez et al., 2014, among others), and the increased skill of this method compared to continuous runs has been reported (Lo et al., 2008). A major advantage of this nesting method is its simplicity. However, it has the undesirable side effect of producing a large number of independent simulations, each of which requiring a spin-up period that has to be discarded. In this study we test this approach by simulating every single day independently, with a spin-up period of 12 h for each run.

A more sophisticated method is to force the RCM to follow the driving large-scale conditions. This is implemented by additional terms in the dynamic equations that restrict the degrees of freedom of the simulation. This is the so-called nudging nesting, of which two versions are available. The 3-D analysis nudging introduces a Newtonian relaxation term in the prognostic equations of the model, and was first introduced by Charney et al. (1969). This addition corrects some variables by an artificial tendency term based on the difference between the original state produced by the model and the driving dataset (Lo et al., 2008). WRF provides a number of options that allow selecting which variables and vertical levels should be affected by the correction term. In the current study, horizontal wind, temperature and humidity are nudged in every level but in the boundary layer. The intensity of the correction depends on a nudging factor, which is set here to the default value of $3 \times 10^{-4}\,s^{-1}$, which is also used in similar studies (Lo et al., 2008).

GMDD
8, 5437–5479, 2015

A variation of this method is spectral nudging, introduced by von Storch et al. (2000). In this approach the variables are Fourier-transformed prior to the nudging. Then, only selected parts of the spectrum are nudged in a similar fashion as the 3-D analysis nudging approach, i.e., by introducing a Newtonian relaxation term in the equations. In doing so, the model is forced to mimic the long waves of the driving input data, which contain the large-scale pattern of the atmospheric circulation, whereas it is free to add value in the smaller scales (Miguez-Macho et al., 2005). As in the sensitivity experiments using 3-D analysis nudging, the simulations carried out in this study nudge horizontal wind, temperature and humidity only in the levels above the PBL, and with the same nudging factors, $3 \times 10^{-4}\,\mathrm{s}^{-1}$. Unlike 3-D analysis nudging, this configuration requires setting the number of waves to be considered in the Fourier analysis, which controls the spatial variability from the input dataset that is being preserved. This number is set to 4 and 2 for the domains D1 and D2, respectively, which correspond to a wave length of about 1000 km. Due to their small size, no nudging is applied in the two innermosts domains.

3.4 Overview of the experiments

This section summarises the set of simulations carried out to investigate the sensitivities of the different settings. Following the approach by Etienne et al. (2013), a total of 24 historical wind storms is considered (Table 1). The selected storms appear between November and February and are embedded in different synoptic scale flow conditions. Each storm is simulated using eight different model configurations encompassing the sensitivity due to PBL parameterization, nesting method and horizontal resolution (Table 2). Thus, a total of 192 simulations are performed. Each simulation spans 6 days with the corresponding storm in the middle of the simulation, and discarding a spin-up period of 12 h.

The comparison of observations and simulation results is performed for hourly values at each observational site. For this, the simulation result at the closest grid point to the observational site is selected. Although this can lead to representativeness errors

GMDD
8, 5437–5479, 2015

(Jiménez et al., 2010), such errors are systematic in all simulations, and do not play a significant role in the assessment of the relative model performance across model configurations.

4 Results

4.1 The role of the PBL scheme

To evaluate the sensitivity of the model result due to different PBL schemes, the setups C1 to C4 are compared with each other (Table 2). The analysis concentrates on results of the innermost domain. All storms are analysed in an identical way, but for the sake of brevity most of the discussion is based on the results for storm Lothar (storm number 13 in Table 1). Still, similarities and deviating characteristics found in other storms are discussed subsequent to the analysis of Lothar storm.

Figure 3 shows the situation during the 24 h around the most mature phase of storm Lothar. This situation was characterized by a intense upper-level zonal jet and strong baroclinicity. The storm formed over the western Atlantic and moved through the Atlantic with moderate amplitude until it reached the French Atlantic coast. There, it experienced an explosive growth as it travelled poleward across the upper-level jet axis (Rivière et al., 2010). The synoptic scale was dominated by a strong north–south gradient in geopotential height that produced strong large-scale winds with a western component.

The surface winds over Switzerland during storm Lothar are presented in Fig. 4 showing the wind speed averaged over 109 weather stations during a 6-day period. The temporal agreement of the sensitivity simulations with the observations is remarkable. The most severe winds peaked on the 26 December 12:00 UTC, but also the secondary peaks in the time series are generally well captured by all sensitivity simulations. Despite the good timing, an overestimation of wind speed becomes apparent. This overestimation of wind speed is in agreement with the results reported by other

GMDD
8, 5437–5479, 2015

studies in different locations and synoptic circulations (Cheng and Steenburgh, 2005; Mass and Ovens, 2011; Jiménez and Dudhia, 2012). The comparison of the sensitivity simulations with different PBL schemes (configurations C1 to C4 in Fig. 4) shows that the YSU* scheme (C2) substantially reduces such overestimation of wind speed. The setup showing the strongest overestimation of surface winds is the fully local scheme, MYJ (C3), followed by the hybrid approach, ACM2 (C4). This suggests that the non-local approach used in both the YSU and YSU* schemes is more suited to reproduce wind speed over complex terrain confirming findings of Jiménez and Dudhia (2012).

Figure 4 provides a first glance of the model-observation comparison. Still, many details are lost by averaging over all stations, in particular the evaluation of the model performance to reproduce the spatial distribution of the most severe winds. Therefore, additional statistics are performed which are presented for storm Lothar in Fig. 5. The boxplots and diamonds show the temporal and the spatial performance, respectively (Fig. 5). Thereby, the boxplots represent the distribution of 109 stations for four statistical metrics that evaluate the temporal performance of the simulation: correlation, Root Mean Square Error (RMSE), bias of the mean wind speed and bias of the maximum wind speed. These four metrics are included since they allow evaluating if the model generally tends to over- or under-estimate wind speed, but also if the simulation is able to mimic the temporal evolution. Note that considering the maximum wind speed is important for scientific questions on extremes on wind speed. To assess the spatial skill of the sensitivity simulations (illustrated by diamonds in Fig. 5) the wind speed is averaged over the 6 days of each storm simulation at each location. This is done separately for the model and the observations resulting in two spatial patterns of mean wind. Finally, the spatial correlation, spatial RMSE, and spatial biases are calculated. Note that this calculation is not meaningful for maximum wind speed (therefore omitted).

The temporal metrics (shown by boxplots) resemble the findings of the time series in Fig. 4, showing that all model configurations tend to overestimate wind speed. Compared to other PBL schemes, the YSU* scheme (C2) is able to reduce the bias of the mean wind, although it still shows slight positive biases for more than 75 % of the stations. Additionally, the RMSE is lower in the sensitivity simulation with the YSU* (C2). The temporal correlation ranges between 0.8 and 0.2, depending on the weather station. The median value is about 0.6 in all configurations. There is a rather low variation between the sensitivity simulations in the temporal correlation, since this metric is dominated by the accuracy of the driving dataset, which is common to all simulations. There is however a lower correlation in the C2 configuration compared to the other configurations. This is a consistent feature across different storms (see discussion below). The skill of the maximum wind speed behaves very similar to the mean bias for all sensitivity simulations, although errors become more pronounced: the MYJ scheme exhibits a strong overestimation of the maximum wind speed that is above 10 $m\,s^{-1}$ for 50 % of the locations, whereas the YSU* scheme simulates values closer to the observations, although with deviations above 3 $m\,s^{-1}$ in 50 % of the locations.

The spatial metrics show that the biases behave similar to the ones of the temporal scale (Fig. 5). This is expected as the spatial bias is identical to the median of the temporal bias if the wind distribution is symmetric. The spatial bias again dominates the spatial RMSE, although in this case the RMSE is significantly lower across all simulations. The sensitivity simulation with the YSU* scheme (C2) shows the lowest spatial RMSE, highlighting the scheme's ability in reducing the overestimation of wind speed. The overall higher spatial correlations than temporal correlations indicate that the model generally is able to simulate the spatial structure of wind independent from the scheme applied. Again, the sensitivity simulation using the YSU* scheme is superior in this metric. Interestingly, the spatial correlation when using this scheme contrasts with the sensitivity simulation with original YSU scheme (C1), as the latter ranks worst among all sensitivity simulations with respect to the PBL scheme. Thus, the spatial metrics show that the YSU* scheme of Jiménez and Dudhia (2012) improves the surface wind simulation by taking into account unresolved orography.

Next, the sensitivity of the model to the PBL scheme is assessed with respect to wind direction. Thereby, the wind rose of the storm Lothar is shown (Fig. 6). The synoptic situation of storm Lothar shows a very intense westerly flow (Fig. 3). As expected, this

GMDD
8, 5437–5479, 2015

situation dominates the wind rose showing primarily south-western directions at the surface. There are additional peaks in the observations in other directions, although due to the pooling process, it could be due to a systematic biases in certain stations (typically valleys, where the 2 km resolution could not be sufficient and lead to representativity errors), rather than a general change in wind direction during the life-time of the storm. Regardless of the PBL scheme, the simulations of storm Lothar are able to capture the main wind direction with a slight systematic bias towards southern directions. The major difference among configurations is a slightly less pronounced preferred direction in the YSU* scheme, although it does not contribute to reduce the southern bias. Thus, the simulation of wind direction seems to be mostly insensitive to the PBL scheme selected.

Most of the conclusions drawn from the analysis of the storm Lothar about the PBL schemes are consistent through the various storms simulated. This is illustrated in a comprehensive although summarised way in Fig. 7. Hereby, the "temporal" series show the median temporal correlation (i.e., the centre of the boxplots in Fig. 5) whereas "spatial" series indicate the mean spatial correlation (i.e., the diamonds in Fig. 5). The temporal correlation seems to be mostly insensitive to the choice of PBL scheme (C1 to C4 in Fig. 7a) with the exception of the YSU* scheme (configuration C2), which shows a slightly lower temporal correlation for almost all storms. Although the authors could not find reasons for the reduced temporal correlation, this phenomenon becomes ameliorated when nudging is used (see next section), rendering this caveat less relevant for the sake of the identification a suitable model setup. Still, the reduction of the overestimation of wind speed by this configuration leads to lower temporal RMSE across the storms (Fig. 7b). This improvement becomes especially noticeable in the maximum wind speed bias (Fig. 7c) where the sensitivity simulations with the YSU* scheme show that the bias fluctuates around zero whereas it is significantly larger for the other setups (C1, C3, and C4). In space, the comparison of the PBL schemes demonstrates that the YSU* scheme exhibits systematically higher spatial correlations (Fig. 7d). Thus, the simulations of all storms using the YSU* scheme are able to better allocate the wind speeds at the right locations than the simulations using other PBL schemes. The simulations using the YSU* scheme further exhibit lower spatial RMSEs, due to higher correlations and a reduction of the overestimation of wind speed (Fig. 7e).

Wind direction performance across all storms is analysed in a similar fashion. However, this variable has to be treated differently, taking into account the problems associated to its circularity. Thus, similarly to Jiménez and Dudhia (2013) the Δd parameter is calculated:

$$\Delta d = \begin{cases} d_{\mathrm{WRF}} - d_{\mathrm{obs}} & \text{if } |d_{\mathrm{WRF}} - d_{\mathrm{obs}}| \leq 180 \\ d_{\mathrm{WRF}} - d_{\mathrm{obs}} - 360 & \text{if } d_{\mathrm{WRF}} - d_{\mathrm{obs}} > 180 \\ d_{\mathrm{WRF}} - d_{\mathrm{obs}} + 360 & \text{if } d_{\mathrm{WRF}} - d_{\mathrm{obs}} < -180. \end{cases}$$

This definition produces positive (negative) biases when simulated wind direction is orientated clockwise (counter-clockwise) with respect to observations. Once this parameter is calculated for each site in each time step, its distribution is obtained. For this, all values are pooled, so the temporal and spatial details are lost in the discussion hereafter. A RMSE that accounts for the deviations between the simulation and the observations in every location and time step for each storm is derived from the distribution of this bias using

$$\mathrm{RMSE} = \left[\frac{1}{n}\sum_{i=1}^{n}(\Delta d_i)^2\right]^{1/2}.$$

The sensitivity simulations show a RMSE of about 70° regardless of the PBL scheme (Fig. 8). Similarly, the median of Δd exhibits a negative bias, again independent from the PBL scheme. For both metrics, the inter-case variation is larger than the variation between the different sensitivity simulations. Thus, this confirms the finding of the storm Lothar that the PBL scheme plays a minor role in reproducing wind direction. Still, it is noteworthy that the C3 and C4 configurations perform better than C1 and C2 as they

GMDD
8, 5437–5479, 2015

exhibit lower Δd and lower RMSE. This result is expected, and in good agreement with the findings by Jiménez and Dudhia (2013), who pointed out that the model's ability to reproduce wind directions is inversely related to wind speed.

To assess whether the results of wind direction and the minor role of the PBL scheme may depend on the storm selected, wind roses of three additional storms are shown in Fig. 6. The storm S07 corresponds to a typical Foehn storm. Unlike for the Lothar storm, the wind rose does not show preferred directions, as expected since Foehn storms affect only part of Switzerland. S16 corresponds to a bise storm. In this configuration there is again a clear preferred direction, but is exactly opposite to Lothar. In this storm there is a clear second maximum towards -30°. Finally, S24 corresponds to the Xynthia storm in February 2010. This is a west-wind storm, although its particular trajectory when traveling towards Switzerland induces a Foehn-like situation, and thus has been catalogued as such by Etienne et al. (2013). In these examples, all sensitivity simulations show remarkable skill in identifying the most dominant wind directions. WRF is clearly able to capture the different nature of these storms, and simulate the surfaces wind regime accordingly. However, none of the four PBL schemes stands out in reproducing the wind direction, resembling the minor role of the PBL scheme and showing that this result is independent from the specific type of the storm.

4.2 The role of the nesting technique

The analysis carried out in the former section indicates that the YSU* scheme is superior compared to the other PBL parameterizations, so this scheme is used in the sensitivity experiments hereafter (see Table 2). The next choice pertains how the RCM is nested to the driving dataset. To assess the sensitivity of nesting approach, the focus is set on the sensitivity simulations C2, C6, C7 and C8, where the free simulations (C2) are compared with analysis nudging (C6), reforecast (C7) and spectral nudging (C8). Figure 4 illustrates that the nesting techniques further reduce the systematic overestimation of the wind in the case of storm Lothar. For the wind speed maxima, the configurations C6 and C7 better reproduce the intensity and precise timing compared to the C2 configuration.

Figure 5 presents spatial and temporal performance metrics for the storm Lothar. Spatially, the sensitivity simulations, which include nudging techniques, exhibit slightly higher correlations than the free simulation (C2). In contrast, the spatial bias show that the analysis nudging reduces bias compared to C2, whereas the reforecast method increases the bias. The latter is due to the last day of the simulation, where this sensitivity simulation exhibits a strong bias (Fig. 4). For the temporal performance metrics, all nudged simulations (C6–C8) tend to increase the correlation compared to C2, although the improvements are small and rise concerns regarding the robustness of this finding. A more clear improvement introduced by nudging is however found for the maximum wind. The original YSU* scheme without nudging shows systematic positive biases in this variable, which are reduced when reforecast, but especially analysis or spectral nudging, are used (Fig. 5).

The analysis of wind direction delivers similar results as in the sensitivity to different PBL schemes (Fig. 6). The role of the nudging approach in correctly simulating the wind direction is minor regarding the storm Lothar. So, it is not possible to identify any nesting configuration that outperforms the others. Instead, all simulations behave similarly, and the main wind direction seems to be equally reproduced across sensitivity simulations according to the synoptic characteristic of the storm.

As before the analysis is extended to all 24 storms. The mean temporal correlation obtained for different storms is shown in Fig. 7a. This figure illustrates that the temporal agreement is slightly but consistently improved when some nudging is applied, rendering the temporal agreement with the observations comparable to the other schemes, as argued for the storm Lothar. The analysis and spectral nudging (C6 and C8) systematically improve the simulations compared to the free simulation (C2). The reforecast (C7) exhibits the improvement of temporal correlation to be highly dependent on the storm considered. This becomes even more obvious in Fig. 7c where the C6 and C8 schemes exhibit lower RMSE than C2, and also generally lower RMSE than C7.

GMDD
8, 5437–5479, 2015

Moreover, nudging reduces the bias in maximum wind speed consistently, and makes analysis and spectral nudging equally suitable to improve the maximum wind speed compared to free simulations (C2). Regarding the improvement in wind direction the model performance varies erratically depending on the storm (Fig. 8). The role of the nesting scheme with respect to the median error Δd is even smaller than of the PBL schemes. A very similar result can be drawn from the analysis of the RMSE, although in this case the nesting setups generally exhibit lower RMSE than the free simulation. However, these differences between the schemes are small, so that an identification of a nesting setup that significantly outperforms the others is not possible when considering wind direction.

4.3 The role of horizontal resolution

As argued above, the horizontal resolution has a profound impact on the ability of the model to simulate wind speed. In particular this is the case if the closest grid point of the model to the weather station is used in the analysis. We note that this simple approach neglects the fact that the model averages subgrid terrain properties, and leads to so-called representativity errors. It is beyond the scope of this study to assess these errors and to address a method to minimise them, since they introduce systematic biases that only depend on the domain configuration, which is fixed across simulations, and thus play a secondary role in the evaluation of the relative skill of different model configurations. Still, such errors, and the model performance in general, depend on the model resolution, so the importance of model resolution and the type of station is discussed in more detail.

The representativity error is quantified by calculating the horizontal distance s and difference of height Δh between the stations and the closest grid point (identical to the model skill assessment above). The mean representativity error over all weather stations as well as the standard deviation are given in Table 3 for the domains D2 to D4 with resolutions of 18, 6 and 2 km, respectively. Obviously the 2 km resolution is closest to the real locations of the observations, with an average distance of 747 m.

The horizontal errors become more severe when a coarser resolution is implemented, and reach a mean of about 6.6 km in the 18 km resolution setup. As expected, the height bias is close to zero, but there is a large standard deviation from station to station, indicating that the error is pronounced in areas of complex topography. The model topography is too smooth even at 2 km grid size and lacks to reproduce the real topography, which explains the high standard deviations.

The influence of the horizontal resolution on the model performance is investigated using the C6 configuration as an example (Fig. 9). Considering all stations, spatial correlations are 0.74, 0.39 and 0.22 for the resolutions from 2, 6 to 18 km, respectively. Similarly, the bias increases from 0.46, 2.19 and 3.24, respectively. This increase in bias is explained by the fact that a coarser resolution implies smoother orography, which eventually leads to an excess of wind speed due to the underestimated terrain roughness. The smoothness is also a reason why the RMSE monotonously increases.

For temporal metrics, a somewhat unexpected behaviour is found. Although the temporal correlation drops to a median value of zero in the coarsest domain analysed, the model exhibits a remarkable high correlation in the 6 km resolution domain. To better understand this high correlation the site-averaged wind speed in different domains for the case Lothar is compared to observations (Fig. 10). Although the series corresponding to D4 is more realistic and reproduces the timing and intensity of the most severe wind speed, the simulation in 6 km (D3) captures the phasing of secondary peaks in the time series better than in the 2 km resolution. Indeed, the RMSE reproduces the expected result of a reduction in performance when successive coarser domains are used, and demonstrates that the use of several statistics allows more robust assessments of the model performance.

The role of the representativity error is explored through the separation of the observational sites in subcategories such as stations in plains, mountain or valleys, as shown in Fig. 9 labelled PL, MO and VA, respectively. Although the temporal correlation is not dramatically dependent on the geographical category, it is slightly higher over plains, as expected by the fact that the model resolution is more suitable for simple terrain, and it is worse over valleys, where important terrain features remain unresolved. The performance measurements behave similar in D3, when separating in PL, MO and VA. In D2 the correlation is too low that it precludes drawing any conclusion. Although biases are generally close to zero in the innermost domain, there is a larger variation between the stations in the mountains, because the differences between the station height and model topography can be large and indeed the RMSE is significantly larger in this locations.

The spatial correlation in the innermost domain shows a low value of 0.31 over the plains, which contrasts with the value of 0.78 obtained for mountains. This can be explained as a signal-to-noise artefact. The problem is that in the plains the mean wind is not as strongly modulated by height as it is in mountains, where there is a larger difference among stations. Thus, small variations in mean wind lead to large variations in the spatial correlation, since the mean wind speed is not a good predictor of the location of a station within plains. Additionally, the correlation is calculated according to only the 46 stations that corresponds to the plains in the Lothar storm. Such low number leads to a large variance of the estimator of correlation, which further contributes to the signal-to-noise problem. Thus, the spatial correlation of mean wind patterns over homogeneous terrain is not a meaningful measure of model skill and should be treated with care.

5 Summary and conclusions

This paper analyses a number of sensitivity experiments aimed at identifying a model setup for WRF that minimises systematic errors in hindcast simulations of wind over areas of complex topography. The simulations use the Era-Interim reanalysis for initial and boundary conditions. These data are downscaled to a resolution of 2 km over the Alps in a series of consecutive nested domains. Due to the high demand of computational resources, the analysis is based on case studies, rather than continuous simulations over several years. Therefore, 24 different simulations lasting 6 days and con-

GMDD
8, 5437–5479, 2015

taining prominent historical storms in Switzerland (Etienne et al., 2013) are simulated and analysed. This selection is motivated by their relevance in risk assessments and impact studies, which are two typical applications of dynamically downscaled datasets. To identify a suitable setup to realistically simulate wind over complex terrain, 8 different sensitivity experiments are performed for each case study taking into account different PBL parameterizations, nudging techniques and horizontal resolutions.

The sensitivity tests designed to evaluate the role of the PBL parameterization show that WRF systematically overestimates wind speed compared to observations. The overestimation occurs in all types of location (plains, valleys or mountains), and is exacerbated in coarser domains. This result confirms previous studies pointing out the overestimation of wind speed in simulations with WRF and its relation with unresolved topograhy (e.g Cheng and Steenburgh, 2005; Mass and Ovens, 2011; Jiménez and Dudhia, 2012). For the MYJ scheme wind speeds that are up to 100 % larger than in the observations are found. The overestimation becomes even stronger when focusing on maximum wind speed, a variable especially relevant in impacts studies. However, this drawback can be significantly reduced by choosing the YSU* scheme which, being based on the non-local YSU scheme, explicitly accounts for unresolved orography. These results resemble findings by Jiménez and Dudhia (2012) and Gonçalves-Ageitos et al. (2015), who tested this PBL parameterization in a small area of relatively complex topography in the North of the Iberian Peninsula and in the Pyrenees, respectively. It is noteworthy that this improvement is not produced by a trivial reduction of wind speed in every location, but this reduction is applied where complexity of topography is more severely underestimated, yielding a remarkable increase in the model's ability to reproduce the spatial structure of wind speed.

The model is qualitatively able to reproduce the leading wind directions generated by very different synoptic conditions. However, the simulations still exhibit systematic biases in wind direction that cannot be improved through a suitable model configuration. Generally, the model performance in reproducing wind direction exhibits little sensitivity to all the evaluated model configurations. Thus, the model performance is dominated

GMDD
8, 5437–5479, 2015

by other factors such as the driving conditions, insufficient resolution, or representativity errors.

Additionally, the sensitivity with respect to the nesting technique is explored by comparing free simulations to analysis and spectral nudging, as well as the so-called re-forecast approach. The use of nudging techniques slightly improves several aspects of the simulation, like reducing the mean wind overestimation discussed above and improving the spatial pattern of mean wind (in particular 3-D analysis nudging). Further, the free simulations generally show a lower temporal agreement with observations than nudged simulations, a feature that is consistent across storms. Analysis nudging yields a significant improvement for maximum wind speed, for which the overestimation is reduced and leads to values closer to zero on average than when no nudging is applied. These results indicate that preserving the large-scale circulation via nudging slightly improves the simulation of wind at regional scales, at least for hindcast simulations where the driving dataset is generally reliable, and whose aim is to be as close to the observations as possible. We note however that for other scientific questions a free simulation setup could be more appropriate, as atmospheric processes and their interactions with regional scale features are able to develop desirable disturbances that add value to RCM simulations. Typical examples are climate change projections (van der Linden and Mitchell, 2009; Gómez-Navarro et al., 2010; Jacob et al., 2013), paleosimulations (Gómez-Navarro et al., 2013) but also classical sensitivity and process studies (Kilic and Raible, 2013; Cipagauta et al., 2014).

Using the setup with analysis nudging and the YSU* scheme the role of the spatial resolution and the representativity error is assessed. As expected horizontal resolution is critical for a realistic wind simulation in very complex terrain. A reduction from 6 to 2 km shows a clear improvement in simulating the mean wind pattern as well as maximum winds. The results for the 18 km configuration show barely any skill, with negligible spatial and temporal correlations. Thus, the overestimation of wind speed becomes exacerbated in coarser resolution domains, further indicating that the main source of wind overestimation is the unresolved orography. Separating in plain, mountain and

GMDD
8, 5437–5479, 2015

valley areas the temporal agreement is slightly higher over flat terrain, and reduced in valleys. The mean biases are similar, although showing more spatial variability in the mountains, driven by the larger variability of height biases. More remarkable differences are seen in the RMSE values which show relatively high values of about $6\,\mathrm{m\,s^{-1}}$ in the mountains compared to $3\,\mathrm{m\,s^{-1}}$ in the flat regions and valleys.

In summary, this study suggests two setups depending on the scientific question: (i) the configuration C6 with the YSU* scheme that reduces wind overestimation and increases spatial correlations. It further uses 3-D analysis nudging, that improves the temporal agreement with respect to observations, and at the same time further reduces the overestimation of maximum wind speed and improves the spatial distribution of wind speed. Thus, this combination is the most suitable for running hindcast simulations aimed at achieving a reliable surface wind simulation over areas of complex orography. (ii) When the timing is not so relevant but an undisturbed development of regional processes is needed, the configuration using the YSU* scheme and free simulations delivers a realistic simulation of surface winds over complex terrain.

Acknowledgements. The authors are grateful for the support provided by the Oeschger Centre for Climate Change Research and the Mobiliar lab for climate risk and natural hazards (Mobilab). Thanks are due to the Swiss National Supercomputing Centre (CSCS) for providing the supercomputing facilities and technical support required to perform the RCM simulations. The ERA-interim reanalysis was kindly provided by the ECMWF. Finally, we would like to thank Martina Messmer for sharing her great knowledge of the Swiss geography and the stimulating discussions.

References

Awan, N. K., Truhetz, H., and Gobiet, A.: Parameterization-induced error characteristics of MM5 and WRF operated in climate mode over the Alpine region: an ensemble-based analysis, J. Climate, 24, 3107–3123, doi:10.1175/2011JCLI3674.1, 2011. 5443

Beniston, M., Stephenson, D. B., Christensen, O. B., Ferro, C. A. T., Frei, C., Goyette, S., Halsnaes, K., Holt, T., Jylhä, K., Koffi, B., Palutikof, J., Schöll, R., Semmler, T., and Woth, K.:

Future extreme events in European climate: an exploration of regional climate model projections, Climatic Change, 81, 71–95, doi:10.1007/s10584-006-9226-z, 2007. 5439

Charney, J., Halem, M., and Jastrow, R.: Use of incomplete historical data to infer the present state of the atmosphere, J. Atmos. Sci., 26, 1160–1163, doi:10.1175/1520-0469(1969)026<1160:UOIHDT>2.0.CO;2, 1969. 5446

Chen, F. and Dudhia, J.: Coupling an advanced land surface–hydrology model with the Penn State–NCAR MM5 modeling system. Part I: Model implementation and sensitivity, Mon. Weather Rev., 129, 569–585, doi:10.1175/1520-0493(2001)129<0569:CAALSH>2.0.CO;2, 2001. 5444

Cheng, W. Y. Y. and Steenburgh, W. J.: Evaluation of surface sensible weather forecasts by the WRF and the Eta models over the Western United States, Weather Forecast., 20, 812–821, doi:10.1175/WAF885.1, 2005. 5445, 5449, 5458

Cipagauta, C., Mendoza, B., and Zavala-Hidalgo, J.: Sensitivity of the surface temperature to changes in total solar irradiance calculated with the WRF model, Geofis. Int., 53, 153–162, doi:10.1016/S0016-7169(14)71497-7, 2014. 5459

Davies, H. C.: A laterul boundary formulation for multi-level prediction models, Q. J. Roy. Meteor. Soc., 102, 405–418, doi:10.1002/qj.49710243210, 1976. 5445

Dee, D. P., Uppala, S. M., Simmons, A. J., Berrisford, P., Poli, P., Kobayashi, S., Andrae, U., Balmaseda, M. A., Balsamo, G., Bauer, P., Bechtold, P., Beljaars, A. C. M., van de Berg, L., Bidlot, J., Bormann, N., Delsol, C., Dragani, R., Fuentes, M., Geer, A. J., Haimberger, L., Healy, S. B., Hersbach, H., Hólm, E. V., Isaksen, L., Kållberg, P., Köhler, M., Matricardi, M., McNally, A. P., Monge-Sanz, B. M., Morcrette, J.-J., Park, B.-K., Peubey, C., de Rosnay, P., Tavolato, C., Thépaut, J.-N., and Vitart, F.: The ERA-Interim reanalysis: configuration and performance of the data assimilation system, Q. J. Roy. Meteor. Soc., 137, 553–597, doi:10.1002/qj.828, 2011. 5441

Dierer, S., de Paus, T., Durante, F., Gregow, E., Lange, B., Lavagnini, A., Strack, M., and Tammelin, B.: Predicting wind speed for wind energy; progress of the WINDENG project, Wind Eng., 29, 393–408, doi:10.1260/030952405775992616, 2005. 5440

Draxl, C., Hahmann, A. N., Peña, A., and Giebel, G.: Evaluating winds and vertical wind shear from Weather Research and Forecasting model forecasts using seven planetary boundary layer schemes, Wind Energy, 17, 39–55, doi:10.1002/we.1555, 2014. 5440

Dudhia, J.: Numerical study of convection observed during the Winter Monsoon Experiment using a mesoscale two-dimensional model, J. Atmos. Sci., 46, 3077–3107, doi:10.1175/1520-0469(1989)046<3077:NSOCOD>2.0.CO;2, 1989. 5444

Etienne, C., Goyette, S., and Kuszli, C.-A.: Numerical investigations of extreme winds over Switzerland during 1990–2010 winter storms with the Canadian Regional Climate Model, Theor. Appl. Climatol., 113, 529–547, doi:10.1007/s00704-012-0800-1, 2013. 5439, 5440, 5444, 5447, 5453, 5458, 5467

García-Díez, M., Fernández, J., Fita, L., and Yagüe, C.: Seasonal dependence of WRF model biases and sensitivity to PBL schemes over Europe, Q. J. Roy. Meteor. Soc., 139, 501–514, doi:10.1002/qj.1976, 2013. 5440, 5443, 5444, 5445, 5446

Gómez-Navarro, J. J., Montávez, J. P., Jimenez-Guerrero, P., Jerez, S., García-Valero, J. A., and González-Rouco, J. F.: Warming patterns in regional climate change projections over the Iberian Peninsula, Meteorol. Z., 19, 275–285, doi:10.1127/0941-2948/2010/0351, 2010. 5440, 5459

Gómez-Navarro, J. J., Montávez, J. P., Jerez, S., Jiménez-Guerrero, P., and Zorita, E.: What is the role of the observational dataset in the evaluation and scoring of climate models?, Geophys. Res. Lett., 39, L24701–L24701, doi:10.1029/2012GL054206, 2012. 5443

Gómez-Navarro, J. J., Montávez, J. P., Wagner, S., and Zorita, E.: A regional climate palaeosimulation for Europe in the period 1500–1990 – Part 1: Model validation, Clim. Past, 9, 1667–1682, doi:10.5194/cp-9-1667-2013, 2013. 5440, 5459

Gonçalves-Ageitos, M., Barrera-Escoda, A., Baldasano, J. M., and Cunillera, J.: Modelling wind resources in climate change scenarios in complex terrains, Renew. Energ., 76, 670–678, doi:10.1016/j.renene.2014.11.066, 2015. 5458

Goyette, S.: Development of a model-based high-resolution extreme surface wind climatology for Switzerland, Nat. Hazards, 44, 329–339, doi:10.1007/s11069-007-9130-5, 2008. 5439

Goyette, S.: Synoptic conditions of extreme windstorms over Switzerland in a changing climate, Clim. Dynam., 36, 845–866, doi:10.1007/s00382-010-0820-4, 2010. 5439

Hong, S. and Lim, J.: The WRF single-moment 6-class microphysics scheme (WSM6), J. Korean Meteorol. Soc., 42, 129–151, 2006. 5444

Jacob, D., Petersen, J., Eggert, B., Alias, A., Christensen, O. B., Bouwer, L. M., Braun, A., Colette, A., Déqué, M., Georgievski, G., Georgopoulou, E., Gobiet, A., Menut, L., Nikulin, G., Haensler, A., Hempelmann, N., Jones, C., Keuler, K., Kovats, S., Kröner, N., Kotlarski, S., Kriegsmann, A., Martin, E., Meijgaard, E. v., Moseley, C., Pfeifer, S., Preuschmann, S., Radermacher, C., Radtke, K., Rechid, D., Rounsevell, M., Samuelsson, P., Somot, S., Soussana, J.-F., Teichmann, C., Valentini, R., Vautard, R., Weber, B., and Yiou, P.: EURO-CORDEX: new high-resolution climate change projections for European impact research, Reg. Environ. Change, 14, 563–578, doi:10.1007/s10113-013-0499-2, 2013. 5440, 5459

Janjić, Z.: Nonsingular implementation of the Mellor–Yamada level 2.5 scheme in the NCEP Meso model, Tech. Rep. Officiale Note 437, National Centers for Environmental Prediction, Washingtong D.C., USA, 2001. 5445

Jerez, S. and Trigo, R. M.: Time-scale and extent at which large-scale circulation modes determine the wind and solar potential in the Iberian Peninsula, Environ. Res. Lett., 8, 044035, doi:10.1088/1748-9326/8/4/044035, 2013. 5440

Jerez, S., Montavez, J. P., Gomez-Navarro, J. J., Lorente-Plazas, R., Garcia-Valero, J. A., and Jimenez-Guerrero, P.: A multi-physics ensemble of regional climate change projections over the Iberian Peninsula, Clim. Dynam., 41, 1749–1768, doi:10.1007/s00382-012-1551-5, 2013. 5440

Jiménez, P. A. and Dudhia, J.: Improving the representation of resolved and unresolved topographic effects on surface wind in the WRF model, J. Appl. Meteorol. Clim., 51, 300–316, doi:10.1175/JAMC-D-11-084.1, 2012. 5444, 5445, 5446, 5449, 5450, 5458

Jiménez, P. A. and Dudhia, J.: On the ability of the WRF model to reproduce the surface wind direction over complex terrain, J. Appl. Meteorol. Clim., 52, 1610–1617, doi:10.1175/JAMC-D-12-0266.1, 2013. 5443, 5452, 5453

Jiménez, P. A., García-Bustamante, E., González-Rouco, J. F., Valero, F., Montávez, J. P., and Navarro, J.: Surface wind regionalization in complex terrain, J. Appl. Meteorol. Clim., 47, 308–325, doi:10.1175/2007JAMC1483.1, 2008. 5440

Jiménez, P. A., González-Rouco, J. F., García-Bustamante, E., Navarro, J., Montávez, J. P., de Arellano, J. V.-G., Dudhia, J., and Muñoz-Roldan, A.: Surface wind regionalization over complex terrain: evaluation and analysis of a high-resolution WRF simulation, J. Appl. Meteorol. Clim., 49, 268–287, doi:10.1175/2009JAMC2175.1, 2010. 5440, 5443, 5448

Jiménez, P. A., Dudhia, J., González-Rouco, J. F., Navarro, J., Montávez, J. P., and García-Bustamante, E.: A revised scheme for the WRF surface layer formulation, Mon. Weather Rev., 140, 898–918, doi:10.1175/MWR-D-11-00056.1, 2012. 5443

Kain, J. S.: The Kain–Fritsch convective parameterization: an update, J. Appl. Meteorol., 43, 170–181, doi:10.1175/1520-0450(2004)043<0170:TKCPAU>2.0.CO;2, 2004. 5444

Kilic, C. and Raible, C. C.: Investigating the sensitivity of hurricane intensity and trajectory to sea surface temperatures using the regional model WRF, Meteorol. Z., 22, 685–698, doi:10.1127/0941-2948/2013/0472, 2013. 5459

Kjellström, E., Bärring, L., Jacob, D., Jones, R., Lenderink, G., and Schär, C.: Modelling daily temperature extremes: recent climate and future changes over Europe, Climatic Change, 81, 249–265, doi:10.1007/s10584-006-9220-5, 2007. 5439, 5440

Kotlarski, S., Keuler, K., Christensen, O. B., Colette, A., Déqué, M., Gobiet, A., Goergen, K., Jacob, D., Lüthi, D., van Meijgaard, E., Nikulin, G., Schär, C., Teichmann, C., Vautard, R., Warrach-Sagi, K., and Wulfmeyer, V.: Regional climate modeling on European scales: a joint standard evaluation of the EURO-CORDEX RCM ensemble, Geosci. Model Dev., 7, 1297–1333, doi:10.5194/gmd-7-1297-2014, 2014. 5439

Kwun, J. H., Kim, Y.-K., Seo, J.-W., Jeong, J. H., and You, S. H.: Sensitivity of MM5 and WRF mesoscale model predictions of surface winds in a typhoon to planetary boundary layer parameterizations, Nat. Hazards, 51, 63–77, doi:10.1007/s11069-009-9402-3, 2009. 5440, 5443, 5444

Lo, J. C.-F., Yang, Z.-L., and Pielke, R. A.: Assessment of three dynamical climate downscaling methods using the Weather Research and Forecasting (WRF) model, J. Geophys. Res.-Atmos., 113, D09112, doi:10.1029/2007JD009216, 2008. 5444, 5446

Lorente-Plazas, R., Montávez, J. P., Jerez, S., Gómez-Navarro, J. J., Jiménez-Guerrero, P., and Jiménez, P. A.: A 49 year hindcast of surface winds over the Iberian Peninsula, J. Climate, in press, doi:10.1002/joc.4189, 2014a. 5440

Lorente-Plazas, R., Montávez, J. P., Jiménez, P. A., Jerez, S., Gómez-Navarro, J. J., García-Valero, J. A., and Jiménez-Guerrero, P.: Characterization of surface winds over the Iberian Peninsula, Int. J. Climatol., 35, 1007–1026, doi:10.1002/joc.4034, 2014b. 5442

Mass, C. and Ovens, D.: Fixing WRF's high speed wind bias: A new subgrid scale drag parameterization and the role of detailed verification, in: 24th Conf. on Weather and Forecasting/20th Conf. on Numerical Weather Prediction, vol. 9B.6, Amer. Meteor. Soc., available at: http://ams.confex.com/ams/91Annual/webprogram/Paper180011.html (last access: 8 July 2015), 2011. 5445, 5449, 5458

Mellor, G. L. and Yamada, T.: Development of a turbulence closure model for geophysical fluid problems, Rev. Geophys., 20, 851–875, doi:10.1029/RG020i004p00851, 1982. 5445

GMDD
8, 5437–5479, 2015

Sensitivity of WRF to reproduce surface wind over complex terrain

J. J. Gómez-Navarro et al.

Title Page
Abstract | Introduction
Conclusions | References
Tables | Figures
◂◂ | ▸▸
◂ | ▸
Back | Close
Full Screen / Esc
Printer-friendly Version
Interactive Discussion

Menendez, M., García-Díez, M., Fita, L., Fernández, J., Méndez, F. J., and Gutiérrez, J. M.: High-resolution sea wind hindcasts over the Mediterranean area, Clim. Dynam., 42, 1857–1872, doi:10.1007/s00382-013-1912-8, 2014. 5440, 5443, 5444, 5446

Miguez-Macho, G., Stenchikov, G. L., and Robock, A.: Spectral nudging to eliminate the effects of domain position and geometry in regional climate model simulations, J. Geophys. Res.-Atmos., 109, D13104, doi:10.1029/2003JD004495, 2004. 5444

Miguez-Macho, G., Stenchikov, G. L., and Robock, A.: Regional climate simulations over North America: interaction of local processes with improved large-scale flow, J. Climate, 18, 1227–1246, doi:10.1175/JCLI3369.1, 2005. 5445, 5447

Mlawer, E. J., Taubman, S. J., Brown, P. D., Iacono, M. J., and Clough, S. A.: Radiative transfer for inhomogeneous atmospheres: RRTM, a validated correlated-k model for the longwave, J. Geophys. Res.-Atmos., 102, 16663–16682, doi:10.1029/97JD00237, 1997. 5444

MunichRe: Winter storms in Europe (II) – Analysis of 1999 losses and loss potentials, Munich Reinsurance Company, available at: www.munichre.com (last access: 9 July 2015), 2001. 5439

Muskulus, M. and Jacob, D.: Tracking cyclones in regional model data: the future of Mediterranean storms, Adv. Geosci., 2, 13–19, doi:10.5194/adgeo-2-13-2005, 2005. 5439

Pleim, J. E.: A combined local and nonlocal closure model for the atmospheric boundary layer. Part I: Model description and testing, J. Appl. Meteorol. Clim., 46, 1383–1395, doi:10.1175/JAM2539.1, 2007a. 5445

Pleim, J. E.: A combined local and nonlocal closure model for the atmospheric boundary layer. Part II: Application and evaluation in a mesoscale meteorological model, J. Appl. Meteorol. Clim., 46, 1396–1409, doi:10.1175/JAM2534.1, 2007b. 5445

Rajczak, J., Pall, P., and Schär, C.: Projections of extreme precipitation events in regional climate simulations for Europe and the Alpine Region, J. Geophys. Res.-Atmos., 118, 3610–3626, doi:10.1002/jgrd.50297, 2013. 5439, 5440

Rivière, G., Arbogast, P., Maynard, K., and Joly, A.: The essential ingredients leading to the explosive growth stage of the European wind storm Lothar of Christmas 1999, Q. J. Roy. Meteor. Soc., 136, 638–652, doi:10.1002/qj.585, 2010. 5448

Santos-Alamillos, F. J., Pozo-Vázquez, D., Ruiz-Arias, J. A., Lara-Fanego, V., and Tovar-Pescador, J.: Analysis of WRF model wind estimate sensitivity to physics parameterization choice and terrain representation in Andalusia (Southern Spain), J. Appl. Meteorol. Clim., 52, 1592–1609, doi:10.1175/JAMC-D-12-0204.1, 2013. 5440, 5443, 5444

Schär, C., Vidale, P. L., Lüthi, D., Frei, C., Häberli, C., Liniger, M. A., and Appenzeller, C.: The role of increasing temperature variability in European summer heatwaves, Nature, 427, 332–336, doi:10.1038/nature02300, 2004. 5439

Schiesser, H. H., Pfister, C., and Bader, J.: Winter storms in Switzerland North of the Alps 1864/1865–1993/1994, Theor. Appl. Climatol., 58, 1–19, doi:10.1007/BF00867428, 1997. 5439

Skamarock, W. C., Klemp, J. B., Dudhia, J., Gill, D. O., Barker, D. M., Wang, W., and Powers, J. G.: A description of the advanced research WRF version 3, Tech. Rep. TN–475+STR, National Center for Atmospheric Research, Boulder, CO, USA, 2008. 5443

Staniforth, A.: Regional modeling: a theoretical discussion, Meteorol. Atmos. Phys., 63, 15–29, doi:10.1007/BF01025361, 1997. 5445

Stensrud, D. J.: Parameterization Schemes: Keys to Understanding Numerical Weather Prediction Models, 1st edn., Cambridge University Press, Cambridge, UK, 2007. 5444

van der Linden, P. and Mitchell, J. (Eds.): ENSEMBLES: Climate Change and its Impacts: Summary of Research and Results from the ENSEMBLES Project, Met Office Hadley Centre, FitzRoy Road, Exeter EX1 3PB, UK, 2009. 5440, 5459

von Storch, H. and Weisse, R.: Regional storm climate and related marine hazards in the Northeast Atlantic, in: Climate Extremes an Society, edited by: Diaz, H. F. and Murnane, R. J., Cambridge Unviersity Press, Cambridge, p. 54–73, 2008. 5439

von Storch, H., Langenberg, H., and Feser, F.: A spectral nudging technique for dynamical downscaling purposes, Mon. Weather Rev., 128, 3664–3673, doi:10.1175/1520-0493(2000)128<3664:ASNTFD>2.0.CO;2, 2000. 5447

Welker, Ch., Martius, O., Stucki, P., Bresch, D., Dierer, S., and Brönnimann, S.: Modelling economic losses of historic and present-day high-impact winter windstorms in Switzerland, Tellus A., submitted, 2015. 5439

Whiteman, C. D.: Mountain Meteorology: Fundamentals and Applications, Oxford University Press, New York, 2000. 5439

Title Page
Abstract | Introduction
Conclusions | References
Tables | Figures
◂◂ | ▸▸
◂ | ▸
Back | Close
Full Screen / Esc
Printer-friendly Version
Interactive Discussion

Table 1. List of 24 historical wind storms and the prevailing synoptic flow conditions. This list is adapted from Table 1 in Etienne et al. (2013).

Storm (given name)	Date	Synoptic flow
S01 (Vivian)	27 Feb 1990	Westerly flow
S02	21 Dec 1993	Westerly flow
S03	28 Jan 1994	Westerly flow
S04	26 Jan 1995	Westerly flow
S05	16 Feb 1995	Westerly flow
S06	13 Feb 1996	Westerly flow
S07	11 Nov 1996	Southerly flow (Foehn)
S08	13 Feb 1997	Westerly flow
S09	17 Dec 1997	Southerly flow (Foehn)
S10	05 Jan 1998	Westerly flow
S11	19 Jan 1998	Westerly flow
S12	12 Dec 1999	Westerly flow
S13 (Lothar)	26 Dec 1999	Westerly flow
S14	16 Feb 2000	Westerly flow
S15	06 Nov 2000	Southerly flow (Foehn)
S16	14 Dec 2001	North-easterly flow (Bise)
S17	02 Jan 2003	Westerly flow
S18	12 Jan 2004	Westerly flow
S19	23 Nov 2005	North-easterly flow (Bise)
S20	01 Jan 2007	Westerly flow
S21	03 Dec 2007	Westerly flow
S22 (Klaus)	23 Jan 2009	Westerly flow
S23	10 Feb 2009	Westerly flow
S24 (Xynthia)	28 Feb 2010	Southerly flow (Foehn)

GMDD
8, 5437–5479, 2015

Table 2. Summary of the eight model configurations used in the sensitivity studies.

Configuration	PBL scheme	Nesting
C1	YSU	Free run
C2	YSU*	Free run
C3	MYJ	Free run
C4	ACM2	Free run
C5	YSU	3-D Analysis
C6	YSU*	3-D Analysis
C7	YSU*	Reforecast
C8	YSU*	Spectral

GMDD

8, 5437–5479, 2015

Table 3. Representativity error in different model domains. The mean and standard deviation of the horizontal distance s between the station and the closest grid point and height difference between both Δh (both in meters) is shown for the domains D2 to D4. The values are calculated considering all stations shown in Fig. 1.

	$\overline{s}$	$\sigma(s)$	$\overline{\Delta h}$	$\sigma(\Delta h)$
D2	6592	2392	−139.76	660.49
D3	2075	801	−106.97	537.44
D4	747	296	−2.37	322.33

GMDD
8, 5437–5479, 2015

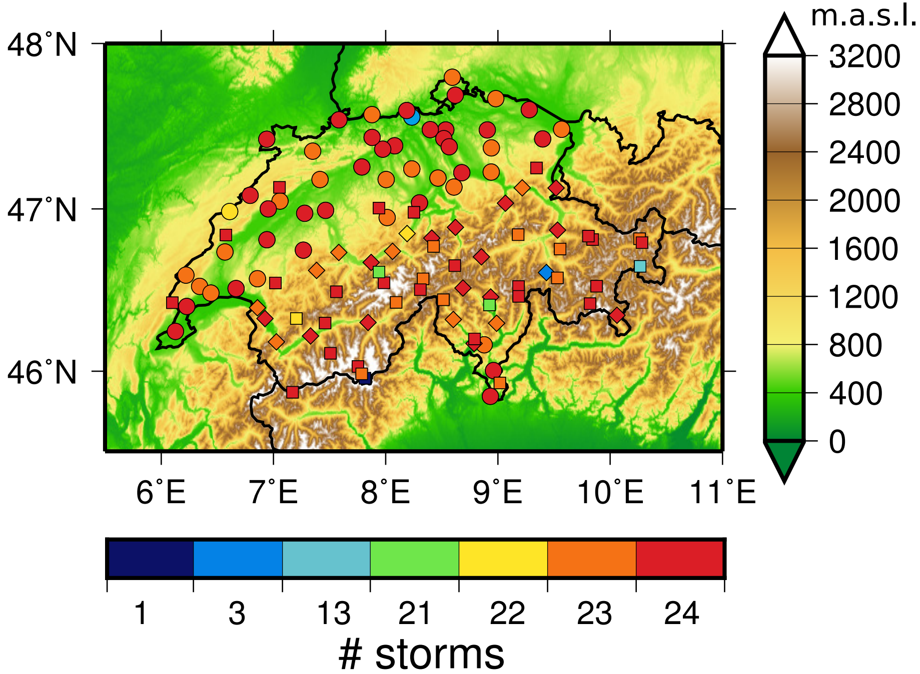

Figure 1. Network of observational sites for wind speed and direction run by MeteoSwiss. The orography of the area is illustrated by the color shading, whereas each symbol indicates the location of an observational site. The filling colour of the symbols indicates the number of storms (Table 1) entering the analysis that are registered by each station. Symbol shape indicates whether the stations are on a plain (circle), a mountain (square) or in a valley (diamond).

GMDD
8, 5437–5479, 2015

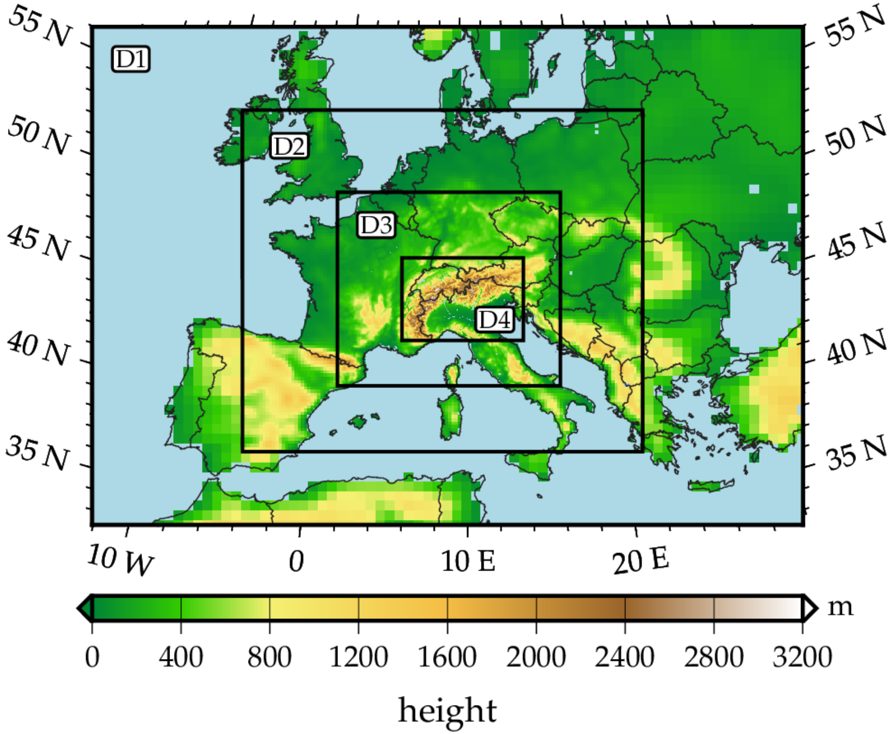

Figure 2. Configuration of the four two-way nested domains. The spatial resolutions are 54, 18, 6 and 2 km, for the domains D1 to D4, respectively. The figure depicts the actual orography and land mask implemented in the simulations.

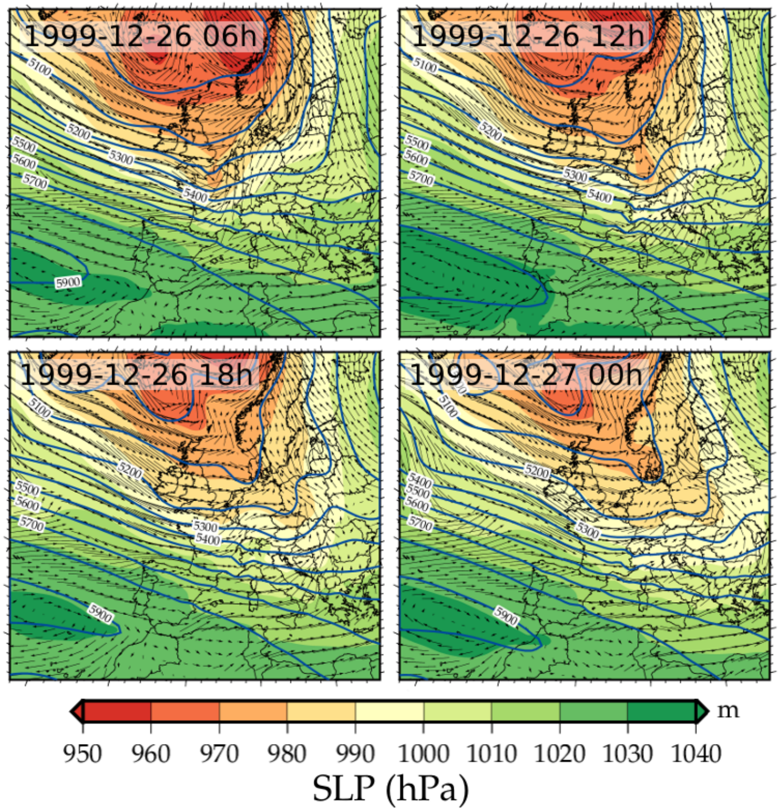

Figure 3. Synoptic situation of the storm Lothar: colour shading depicts the sea level pressure, whereas blue contours indicate the geopotential height at 500 hPa. The arrows represent 10 m s^{-1} wind. The fields represent consecutive snapshots for the period of most severe wind speeds between 26 December, 06:00 UTC and 27 December, 00:00 UTC in steps of 6 h (see Fig. 4). The data fields are obtained from the Era-Interim reanalysis, the same used to drive the RCM simulations.

GMDD
8, 5437–5479, 2015
Sensitivity of WRF to reproduce surface wind over complex terrain
J. J. Gómez-Navarro et al.

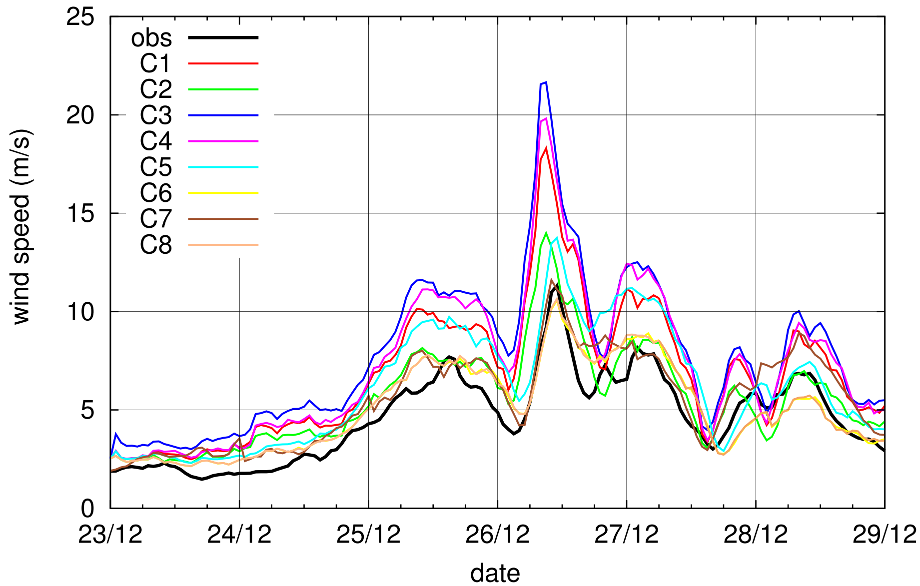

Figure 4. Time series of wind speed for a 6-day period around storm Lothar averaged for 109 stations. Thick black line depicts the series corresponding to the observations, whereas the coloured lines correspond to the simulation results with different model setups (Table 2).

GMDD
8, 5437–5479, 2015

Sensitivity of WRF to reproduce surface wind over complex terrain

J. J. Gómez-Navarro et al.

Title Page
Abstract Introduction
Conclusions References
Tables Figures
◀| |▶
◀ ▶
Back Close
Full Screen / Esc
Printer-friendly Version
Interactive Discussion

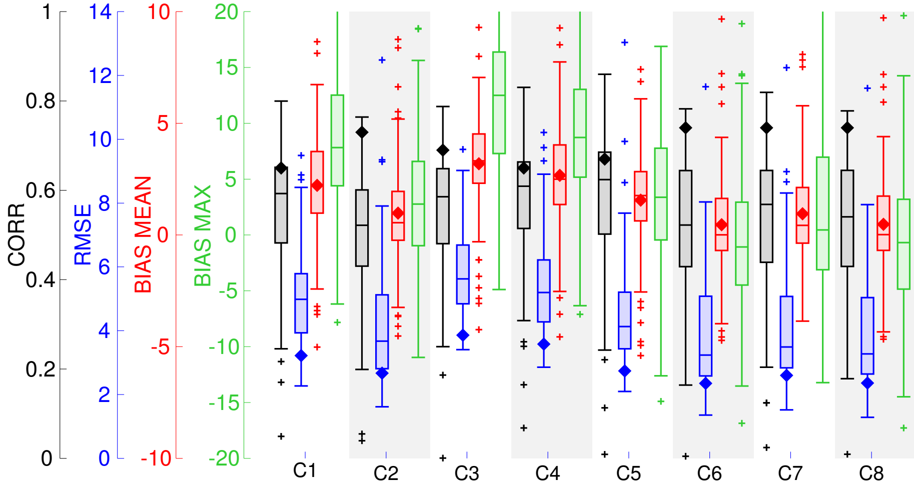

Figure 5. Different skill metrics for the comparison of observations and simulation results for storm Lothar. Each column represents the results of one sensitivity simulation in Table 2. The temporal skill is illustrated by boxplots which represent the distribution of four metrics over 109 weather stations: correlation (black), RMSE (blue), model-observation mean bias (red) and model-observation maximum bias (green). Four different scales are employed, which match the different colours of the symbols. The diamonds represent the spatial skill. They are calculated for the mean wind speed of each location. The boxes represent the second and third quartiles, whereas the whiskers extend from the ends of the box to the most distant point whose y value lies within 1.5 times the interquartile range. Outliers are depicted by crosses.

GMDD
8, 5437–5479, 2015

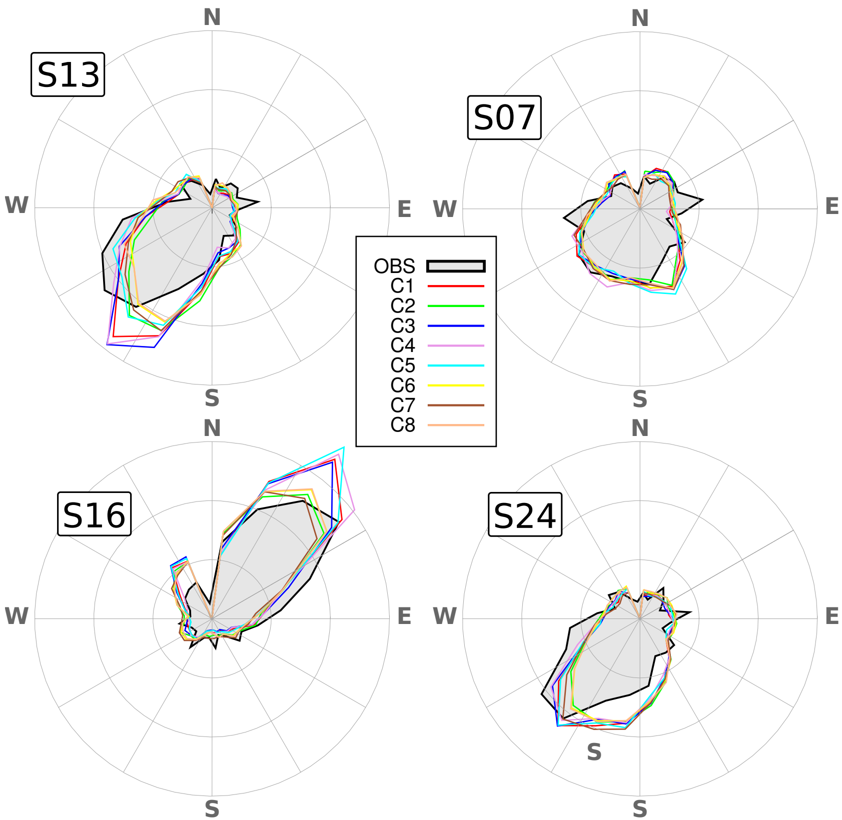

Figure 6. Wind roses corresponding to four different storm cases selected from Table 2. The number of the case is indicated in each panel, and corresponds to storm Lothar (S13), as well as other three storms with different synoptic conditions. The colours correspond to observations and simulations as in Fig. 4. For the calculation of the histograms the hourly wind direction during the entire period registered in each location is pooled, and the number of times that a wind direction lies within each 15° bin is counted and finally normalised.

GMDD
8, 5437–5479, 2015

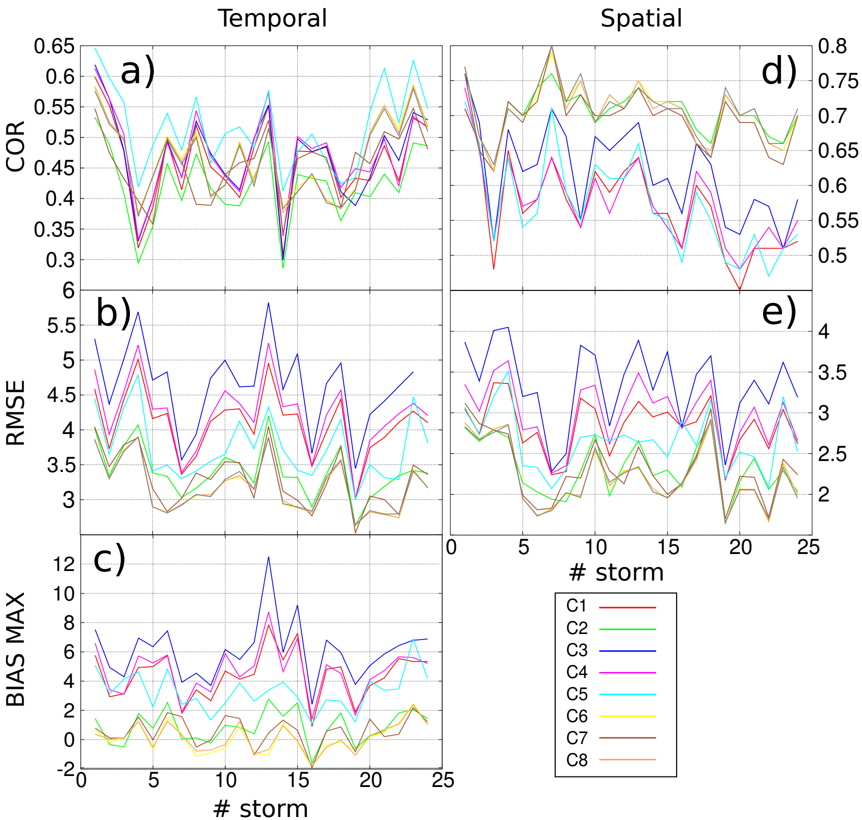

Figure 7. Model performance for the comparison of observed and simulated wind speed across the 24 storms defined in Table 1. Each coloured line corresponds to a model setup. Correlation (**a** and **d**), RMSE (**b** and **e**) and bias in the maximum wind speed **(c)** are shown on the temporal **(a–c)** and spatial (**d** and **e**) domains, respectively. The spatial values correspond directly to the diamonds in Fig. 5, whereas the time statistics show the median value, this is the centre of the boxplots in the same figure.

GMDD
8, 5437–5479, 2015

Sensitivity of WRF to reproduce surface wind over complex terrain

J. J. Gómez-Navarro et al.

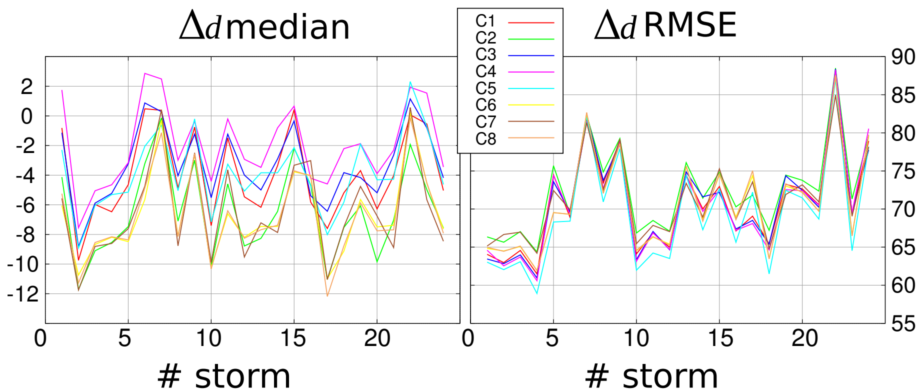

Figure 8. Performance metrics for wind direction for all storms. Left (right) panel shows the model skill evaluated through the median (RMSE) of Δd, as defined in the main text.

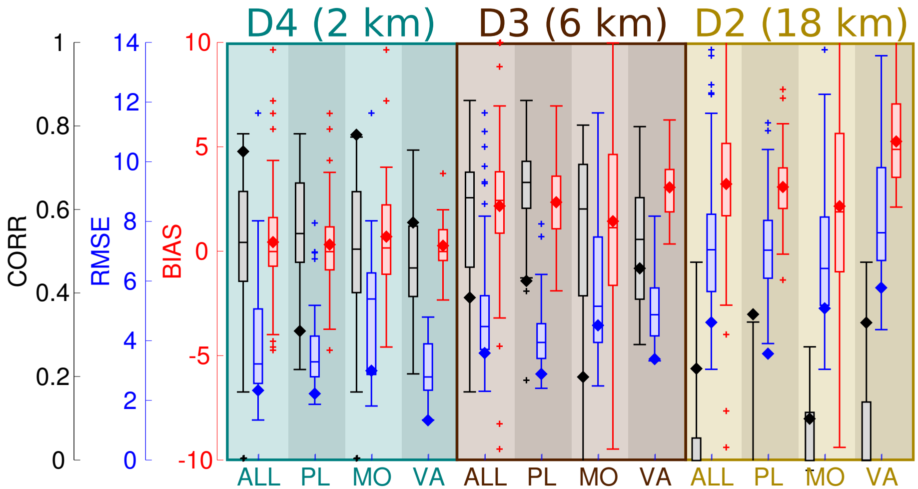

Figure 9. Influence of the grid size for the simulation skill, based on the configuration C6 (Table 2). The figure depicts temporal and spatial correlation, RMSE and bias in a similar way as Fig. 5, but different spatial resolutions (grid size 18, 6 and 2 km in domain D2, D3 and D4) and locations (ALL for all stations; PL for plains; MO for mountains; defined as those locations whose height exceeds 1200 m; and VA for valleys) are shown separately. The locations of each type of station are indicated in Fig. 1.

GMDD
8, 5437–5479, 2015

Sensitivity of WRF to reproduce surface wind over complex terrain

J. J. Gómez-Navarro et al.

Title Page
Abstract | Introduction
Conclusions | References
Tables | Figures
◀| |▶
◀ ▶
Back | Close
Full Screen / Esc
Printer-friendly Version
Interactive Discussion

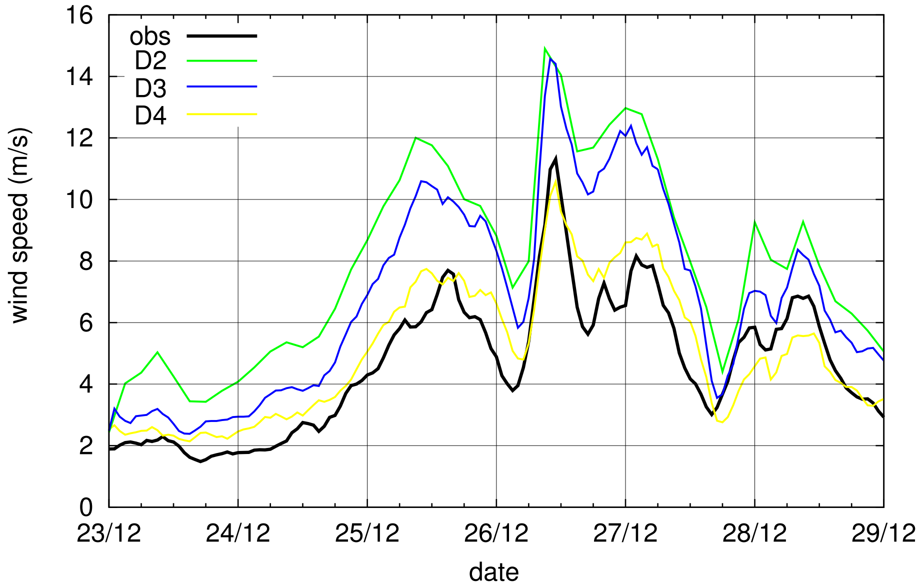

Figure 10. Site-averaged series of wind speed in the 6-day case study containing the storm Lothar. Black and yellow lines correspond to the observations and simulation in the domain D4 corresponding to C6 in Table 2 (same series as in Fig. 4). The green and blue lines correspond to the result with the same model configuration, but in the domains D2 and D3, respectively.

GMDD
8, 5437–5479, 2015